Langmuir
Article
pubs.acs.org/Langmuir

Layer-by-Layer Assembled Multilayer TiO_x for Efficient Electron Acceptor in Polymer Hybrid Solar Cells

Hyunbum Kang,[†] Chanwoo Lee,[⊥] Sung Cheol Yoon,[§] Chul-Hee Cho,[†] Jinhan Cho,*[,‡] and Bumjoon J. Kim*[,†]

[†]*Department of Chemical and Biomolecular Engineering, Korea Advanced Institute of Science and Technology (KAIST), Daejeon 305-701, Korea,* [‡]*Department of Chemical and Biological Engineering, Korea University, Seoul 136-701, Korea,* [§]*Advanced Materials Division, Korea Research Institute of Chemical Technology, Daejeon 305-600, Korea, and* [⊥]*School of Advanced Materials Engineering, Kookmin University, Jeongneung-dong, Seongbuk-gu, Seoul 136-702, Korea*

Received August 13, 2010. Revised Manuscript Received September 15, 2010

We demonstrate that TiO_x nanocomposite films fabricated using electrostatic layer-by-layer (LbL) assembly improve the power conversion efficiency of photovoltaic cells compared to conventional TiO_x films fabricated via the sol−gel process. For this study, titanium precursor/poly(allylamine hydrochloride) (PAH) multilayer films were first deposited onto indium tin oxide-coated glass to produce TiO_x nanocomposites (TiO_xNC). The specific effect of the LbL processed TiO_x on photovoltaic performance was investigated using the planar bilayer TiO_xNC and highly regioregular poly(3-hexylthiophene) (P3HT) solar cells, and the P3HT/LbL TiO_xNC solar cells showed a dramatic increase in power efficiency, particularly in terms of the short current density and fill factor. The improved efficiency of this device is mainly due to the difference in the chemical composition of the LbL TiO_xNC films, including the much higher Ti^{3+}/Ti^{4+} ratio and the highly reactive facets of crystals as demonstrated by XPS and XRD measurement, thus enhancing the electron transfer between electron donors and acceptors. In addition, the grazing incidence wide-angle X-ray scattering (GIWAXS) study revealed the presence of more highly oriented P3HT stacks parallel to the substrate on the LbL TiO_xNC film compared to those on the sol−gel TiO_x films, possibly influencing the hole mobility of P3HT and the energy transfer near and at the interface between the P3HT and TiO_x layers. The results of this study demonstrate that this approach is a promising one for the design of hybrid solar cells with improved efficiency.

Introduction

Hybrid polymer/inorganic nanocomposites have attracted considerable interest due to their applications in various fields such as charge trap nonvolatile memory, catalysts, immunodiagnostic assays, photonic devices, and electrorheological fluids.[1−7] Recently, a great deal of effort has been devoted to the preparation of hybrid photovoltaic devices since conducting polymers and transition metal oxides can be effectively used as organic electron donors and inorganic electron acceptors, respectively.[8−15] Particularly, in photovoltaic devices, the most attractive aspect of using titania (TiO_x) with a conjugated polymer lies in the fact that TiO_x has a low-lying conduction band that accepts electrons easily from almost all organic semiconductors. In addition, the potential to pattern these metal oxides separately makes it easier to increase the interfacial area and the power efficiency. The ability to tune the interfacial properties while maintaining the same donor−acceptor materials provides a means to study the effect of interface modification systematically.[12,14,16−19] Because of these advantages, a number of researchers have prepared TiO_2 layers with ordered or nanoporous structures to improve the power conversion efficiency.[20−22] For example, McGehee group[22] reported that the ordered bulk heterojunction solar cells with nanostructured TiO_x and poly(3-hexylthiophene) (P3HT) had a significantly improved power conversion efficiency because of the increase in the interfacial area and the enhanced charge mobility in the aligned polymer phase compared to a flat reference bilayer device. Kim group[23] also reported that photovoltaic cells

*Corresponding authors. E-mail: bumjoonkim@kaist.ac.kr (B.J.K.); jinhan71@korea.ac.kr (J.C.).

(1) Bockstaller, M. R.; Thomas, E. L. *J. Phys. Chem. B* **2003**, *107*, 10017.
(2) Cheng, J. Y.; Ross, C. A.; Chan, V. Z. H.; Thomas, E. L.; Lammertink, R. G. H.; Vancso, G. J. *Adv. Mater.* **2001**, *13*, 1174.
(3) Kim, B. J.; Fredrickson, G. H.; Hawker, C. J.; Kramer, E. J. *Langmuir* **2007**, *23*, 7804.
(4) Lee, C.; Kim, I.; Shin, H.; Kim, S.; Cho, J. *Langmuir* **2009**, *25*, 11276.
(5) Lee, J. S.; Cho, J.; Lee, C.; Kim, I.; Park, J.; Kim, Y. M.; Shin, H.; Lee, J.; Caruso, F. *Nature Nanotechnol.* **2007**, *2*, 790.
(6) Al Akhrass, S.; Gal, F.; Damiron, D.; Alcouffe, P.; Hawker, C. J.; Cousin, F.; Carrot, G.; Drockenmuller, E. *Soft Matter* **2009**, *5*, 586.
(7) Krishnan, R. S.; Mackay, M. E.; Duxbury, P. M.; Pastor, A.; Hawker, C. J.; Van Horn, B.; Asokan, S.; Wong, M. S. *Nano Lett.* **2007**, *7*, 484.
(8) Beek, W. J. E.; Wienk, M. M.; Janssen, R. A. J. *Adv. Mater.* **2004**, *16*, 1009.
(9) Briseno, A. L.; Holcombe, T. W.; Boukai, A. I.; Garnett, E. C.; Shelton, S. W.; Fréchet, J. M. J.; Yang, P. D. *Nano Lett.* **2010**, *10*, 334.
(10) Coakley, K. M.; McGehee, M. D. *Appl. Phys. Lett.* **2003**, *83*, 3380.
(11) Crossland, E. J. W.; Kamperman, M.; Nedelc, M.; Ducati, C.; Wiesner, U.; Smilgies, D.-M.; Toombes, G. E. S.; Hillmyer, M. A.; Ludwigs, S.; Steiner, U.; Snaith, H. J. *Nano Lett.* **2009**, *9*, 2807.
(12) Goh, C.; Scully, S. R.; McGehee, M. D. *J. Appl. Phys.* **2007**, *101*, 114503/1.
(13) Hal, P. A. v.; Wienk, M. M.; Kroon, J. M.; Verhees, W. J. H.; Slooff, L. H.; Gennip, W. J. H. v.; Jonkheijm, P.; Janssen, R. A. J. *Adv. Mater.* **2003**, *15*, 118.
(14) Lin, Y.-Y.; Chu, T.-H.; Li, S.-S.; Chuang, C.-H.; Chang, C.-H.; Su, W.-F.; Chang, C.-P.; Chu, M.-W.; Chen, C.-W. *J. Am. Chem. Soc.* **2009**, *131*, 3644.
(15) Ma, B. W.; Woo, C. H.; Miyamoto, Y.; Fréchet, J. M. J. *Chem. Mater.* **2009**, *21*, 1413.
(16) Hau, S. K.; Yip, H. L.; Acton, O.; Baek, N. S.; Ma, H.; Jen, A. K. Y. *J. Mater. Chem.* **2008**, *18*, 5113.
(17) Liu, Y.; Scully, S. R.; McGehee, M. D.; Liu, J.; Luscombe, C. K.; Fréchet, J. M. J.; Shaheen, S. E.; Ginley, D. S. *J. Phys. Chem. B* **2006**, *110*, 3257.
(18) Monson, T. C.; Lloyd, M. T.; Olson, D. C.; Lee, Y.-J.; Hsu, J. W. P. *Adv. Mater.* **2008**, *20*, 4755.
(19) Zhu, R.; Jiang, C.-Y.; Liu, B.; Ramakrishna, S. *Adv. Mater.* **2009**, *21*, 994.
(20) Coakley, K. M.; Liu, Y.; McGehee, M. D.; Frindell, K. L.; Stucky, G. D. *Adv. Funct. Mater.* **2003**, *13*, 301.
(21) Wei, Q.; Hirota, K.; Tajima, K.; Hashimoto, K. *Chem. Mater.* **2006**, *18*, 5080.
(22) Williams, S. S.; Hampton, M. J.; Gowrishankar, V.; Ding, I. K.; Templeton, J. L.; Samulski, E. T.; DeSimone, J. M.; McGehee, M. D. *Chem. Mater.* **2008**, *20*, 5229.
(23) Her, H. J.; Kim, J. M.; Kang, C. J.; Kim, Y. S. *J. Phys. Chem. Solids* **2008**, *69*, 1301.

fabricated using ordered TiO_x nanopores were observed to produce more photocurrent than those made from flat titania due to the effective electron acceptance resulting from the increased surface area.

In addition to ordered or nanoporous structures, the power conversion efficiency could also be enhanced by controlling the chemical composition of TiO_x films. This possibility is based on the presence of Ti^{3+} states in thermally annealed TiO_x films. That is, the TiO_x powders prepared by the sol−gel process and the subsequent heating process contain a certain amount of Ti^{3+} surface states that form a donor level between the band gaps of TiO_x, and these states can induce a reduction in the rate of recombination between electrons and holes followed by an increase in photocatalytic activity. Generally, the titanium reduction results from the presence of residual carbon in the layer of organic radicals introduced by titania precursors. After burning during thermal treatment, carbon draws oxygen from the surrounding atmosphere and layer network, leading to the reduction of Ti^{4+} to Ti^{3+}. Therefore, increasing the amount of organic components in the titania precursor layer could increase the fraction of Ti^{3+} states in the TiO_x films formed after thermal annealing, thus improving the photovoltaic properties.

Herein, we show that TiO_x nanocomposite films prepared using electrostatic layer-by-layer (LbL) assembly improve the efficiency of photovoltaic cells compared to conventional TiO_x films prepared via the sol−gel process. The LbL assembly method based on a solution dipping process has been demonstrated to be a versatile and powerful tool for preparing organic and/or inorganic nanocomposite films with tailored optical, electrical, and chemical properties.[4,24−29] Very recently, it was reported that hybrid solar cells based on polythiophene derivatives and CdSe (or PbSe) by the LbL assembly method.[30,31] However, the reported efficiency of the solar cells by the LbL assembly method was extremely low, and thus the advantage of LbL assembly for the fabrication of hybrid solar cells is not demonstrated yet. For our study, titanium precursor/poly(allylamine hydrochloride) (PAH) multilayer films were first deposited onto indium tin oxide (ITO)-coated glass to produce TiO_x nanocomposites (TiO_xNC). The advantage of the LbL TiO_xNC films for use in photovoltaic applications was clearly demonstrated by comparing them with sol−gel processed TiO_x films. To investigate the specific effect of the LbL processed TiO_x on the photovoltaic performance, we adopted the planar type of bilayer TiO_xNC and regioregular poly(3-hexylthiophene) (P3HT) solar cells, which can eliminate complex issues concerning bulk heterojunctions, such as pore filling, phase segregation, and charge collection. In simple bilayer devices, the P3HT/LbL TiO_xNC solar cells showed a dramatic increase in the power conversion efficiency, particular in the short current density and the fill factor. In addition, the two-dimensional (2D) grazing incidence wide-angle X-ray scattering (GIWAXS) study revealed the presence of more highly oriented P3HT stacks on the LbL TiO_xNC film compared to the sol−gel prepared TiO_xNC film, possibly influencing the hole mobility of P3HT and the energy transfer near and at the interface between the P3HT and TiO_x layers. These results demonstrate that this LbL approach is a simple and versatile method for fabricating efficient electron acceptor in polymer hybrid solar cells.

Experimental Section

Preparation of LbL and Sol−Gel TiO_x Nanocomposite Films. The concentration of cationic poly(allylamine hydrochloride) (PAH) (M_w = 70 000, Aldrich) and anionic titanium(IV) bis(ammonium lactato) dihydroxide (TALH) (Aldrich) aqueous solutions used for all the experiments was 1 and 50 mg/mL, respectively. ITO-coated glass substrates had an anionic surface by irradiating UV light. After this procedure, the cationic PAH solution (containing 0.5 M NaCl) was spin-deposited at a fixed rotating speed (typically 4000 rpm) for a short period (about 20 s) until a sufficiently dried film was obtained, and the substrates were then thoroughly rinsed twice at a speed of 4000 rpm with plenty of deionized water. A negatively charged TALH layer was also sequentially deposited onto the substrates using the same procedure as mentioned above. This process was repeated until the desired bilayer number. For LbL TiO_xNC nanocomposite films, the resultant $(PAH/TALH)_n$ multilayer films were thermally annealed at 450 °C for 2 h under nitrogen and additionally annealed at the same temperature for 4 h under oxygen conditions. In this case, the resultant thickness of LbL TiO_xNC film was measured to be about 50 nm as confirmed by ellipsometry. For a control sample, the conventional sol−gel TiO_x films with 50 nm thickness were produced by the sol−gel process using titanium tetraisopropoxide (TIPP) as a precursor and subsequent thermal annealing (450 °C for 2 h under nitrogen and 4 h under oxygen).

Synthesis of Regioregular Poly(3-hexylthiophene) (P3HT). Lithium diisopropylamide (LDA) was generated by addition of *n*-BuLi (1.6 M in hexane, 2.4 mL, 3.84 mmol) to a solution of dry diisopropylamine (0.68 mL, 4.80 mmol) in dry THF (9.1 mL) at −78 °C. The solution was stirred at this temperature for 1 h. The freshly generated LDA solution was added dropwise to 2-bromo-3-hexylthiophene (1.00 g, 4.045 mmol) in dry THF (37.7 mL) at −78 °C. After 1 h reaction at −78 °C, anhydrous $ZnCl_2$ (0.649 g, 4.76 mmol) was added portionwise to the mixture, which was stirred for 30 min and then warmed slowly to RT. Polymerization initiated by addition of $Ni(dppp)Cl_2$ (0.0088 g, 0.016 mmol) to the mixture was carried out at RT for 2 h. The solution was quenched by 0.75 mL of 1.0 N aqueous HCl in order to stop the polymerization. The polymer was precipitated with MeOH (230 mL) containing 2.3 mL of NH_3 7 N in MeOH solution to neutralize it, and the resulting precipitate was then filtered. Oligomers and impurities in the product were removed by Soxhlet extractions with MeOH for 3 h, followed by hexane extraction for 8 h. The polymer was then taken up by Soxhlet extraction with chloroform and isolated by precipitation from chloroform into MeOH. The resulting solid was dried under vacuum to yield the P3HT polymers, resulting in M_n of 16 kg/mol, PDI of 1.3, and regioregularity of 95%. The molecular weights (M_n) and polydispersities (PDI) of the obtained polymers were analyzed by size exclusion chromatography (SEC) using UV and RI detectors and calibrated by polystyrene standards. Additionally, regioregularity (RR) was determined by using H NMR spectroscopy.

Devices Fabrication and Measurements. Two different kinds of TiO_xNC films prepared from sol−gel and LbL assembly were subjected to ultrasonication in different solvent systems including acetone, 2% soap in water, deionized water, and then 2-propanol. Each step was carried out for 20 min. The substrates were then dried under a stream of nitrogen. All procedures after this point were performed in an inert-atmosphere (N_2) glovebox. A solution of P3HT (M_n = 16 kg/mol, PDI = 1.3, RR = 95%) in chlorobenzene (15 mg/mL) was prepared and stirred above 100 °C for more than 24 h to ensure complete dissolution. The solutions were passed through a 0.2 μm poly(tetrafluoroethylene) (PTFE) syringe

(24) Zhang, X.; Shi, F.; Yu, X.; Liu, H.; Fu, Y.; Wang, Z.; Jiang, L.; Li, X. *J. Am. Chem. Soc.* **2004**, *126*, 3064.
(25) Wang, Y.; Tang, Z.; Correa-Duarte, M. A.; Liz-Marzán, L. M.; Kotov, N. A. *J. Am. Chem. Soc.* **2003**, *125*, 2830.
(26) Decher, G. *Science* **1997**, *277*, 1232.
(27) Caruso, F.; Caruso, R. A.; Mohwald, H. *Science* **1998**, *282*, 1111.
(28) Park, J.; Kim, I.; Shin, H.; Lee, M. J.; Kim, Y. S.; Bang, J.; Caruso, F.; Cho, J. *Adv. Mater.* **2008**, *20*, 1843.
(29) Cho, J.; Char, K.; Hong, J. D.; Lee, K. B. *Adv. Mater.* **2001**, *13*, 1076.
(30) McClure, S. A.; Worfolk, B. J.; Rider, D. A.; Tucker, R. T.; Fordyce, J. A. M.; Fleischauer, M. D.; Harris, K. D.; Brett, M. J.; Buriak, J. M. *ACS Appl. Mater. Interfaces* **2010**, *2*, 219.
(31) Zotti, G.; Vercelli, B.; Berlin, A.; Pasini, M.; Nelson, T. L.; McCullough, R. D.; Virgili, T. *Chem. Mater.* **2010**, *22*, 1521.

Scheme 1. Schematic Device Architectures of TiO_x/P3HT Photovoltaic Cells: (a) Sol−Gel TiO_xNC/P3HT System and (b) LbL TiO_xNC/P3HT System

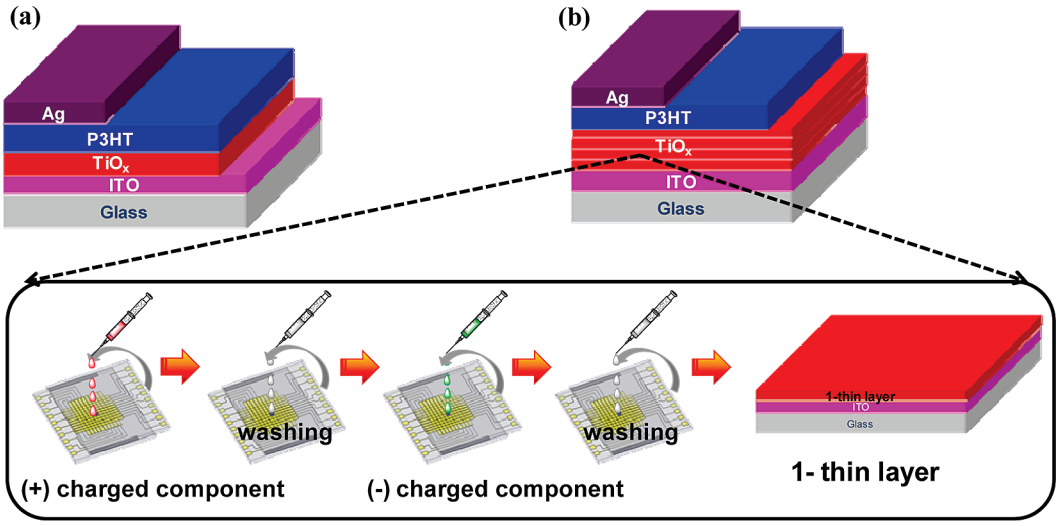

filter, immediately prior to use in the device. Filtered solution was applied onto two different samples of (1) LbL TiO_xNC film and (2) sol−gel TiO_xNC film by spin-casting at 2000 rpm for 40 s to obtain ~50 nm polymer thickness. The substrates were then placed in an evaporation chamber and held under vacuum (high 10^{-6} Torr) for more than 1 h before evaporating 100 nm thick Ag. The configuration of the shadow mask afforded four independent devices on each substrate. Thermal annealing was performed at 120 °C at least 8 h. After Ag deposition, the photovoltaic performances were characterized using a solar simulator (ABET Technologies) with air mass AM 1.5 G filters. Intensity of solar simulator was carefully calibrated using AIST certified silicon photodiode. Current−voltage behavior was measured with a Keithley 2400 SMU. The active area of the fabricated devices was 0.10 cm^2.

QCM Measurement. Quartz crystal microbalance (QCM) device (QCM200, SRS) was used to measure the mass of the material deposited after each adsorption step. The resonance frequency of the QCM electrodes was ~5 MHz. The adsorbed mass of PAH and TALH, Δm, can be calculated from the change in QCM frequency, ΔF, using the Sauerbrey equation: $\Delta F\,(\mathrm{Hz}) = -56.6\Delta m_A$, where Δm_A is the mass change per quartz crystal unit area in micrograms per square centimeter ($\mu g/cm^2$).

AFM Measurement. The surface morphology of sol−gel and LbL TiO_xNC films was examined with an atomic force microscopy (AFM) (Veeco Dimension 3100) in tapping mode.

XPS Measurement. X-ray photoelectron spectroscopy (XPS, Sigma Probe) was performed to investigate the chemical composition of sol−gel and LbL TiO_x NC films.

GIWAXS Measurement. GIWAXS measurement was performed to reveal the 2-dimensional molecular structure of P3HT polymers adjacent to the P3HT/TiO_x interface. Therefore, instead of preparing 50 nm thick P3HT film as used for the device fabrication, thin P3HT films (~10 nm) were spun-cast from 2 mg/mL P3HT solution in chlorobenzene onto two different (1) sol−gel TiO_xNC and (2) LbL TiO_x NC layers. Additionally, for a control sample, another 10 nm P3HT film was made directly onto the Si substrate. All samples were annealed in a N_2-filled glovebox at 120 °C for 8 h. GIWAXS measurements with a X-ray wavelength of 1.3807 Å were performed on beamline 4C.2 in the Pohang Accelerator Laboratory (South Korea). The incidence angle was carefully chosen to allow for complete X-ray penetration into the polymer film. The scattering spectra were collected as the 2D image map that can be divided into a component in the plane of the substrate (q_x) and a component perpendicular to the substrate (q_z).

Results and Discussion

We first prepared TiO_xNC films by the LbL method for application as the electron acceptor in polymer/inorganic hybrid solar cells. The conventional sol−gel TiO_xNC film to act as a control sample was fabricated for comparison with LbL TiO_xNC. The film thickness of the LbL and sol−gel TiO_xNC films was adjusted to be 50 nm. Scheme 1 shows the resultant structure of the inverted polymer/inorganic solar cells and the two different types of TiO_x films employed in this study.

QCM was performed to measure the amount of PAH and TALH adsorbed in the LbL multilayer films. Figure 1a shows the frequency changes, $-\Delta F$, and the mass changes were calculated from the changes in the adsorbed PAH and TALH with increasing numbers of layers. The changes in mass were calculated from the changes in frequency using the Sauerbrey equation (see the Experimental Section). These QCM frequency (or mass) changes suggest that regular multilayer film growth occurs when anionic TALH and cationic PAH are assembled into LbL from deposition solutions. The alternate deposition of PAH and TALH resulted in a $-\Delta F$ of 15 ± 1 (Δm of ~265 ng cm^{-2}) and a $-\Delta F$ of 54 ± 2 ($-\Delta m$ of ~1236 ng cm^{-2}), respectively. This uniform growth of multilayers was also confirmed by the regular increase in absorbance at 243 nm as shown in Figure 1b. The PAH/TALH multilayers were easily converted to TiO_xNC films when annealed at 450 °C, while the PAH (thermal degradation temperature of PAH ≈ 240 °C) and TALH layers underwent thermal degradation. In this case, the thermally decomposed amount of organic components was measured as about 60% (using thermogravimetric analysis). On the other hand, TiO_x precusors (i.e., TIPP) in the sol−gel reaction were thermally annealed at 450 °C to form TiO_x films with a concomitant mass loss of 45% due to the thermal degradation of organics. These results clearly indicated that LbL TiO_xNC was formed by the thermal decomposition of a greater amount of organic components compared to sol−gel TiO_xNC films.

On the basis of these results, we fabricated hybrid solar cells composed of conducting polymers and TiO_x films. In general, crystalline anatase type TiO_x films for use in photovoltaic applications have been prepared by the sol−gel approach in which the titanium precursor is hydrolyzed, followed by sintering at high temperature.[10,12,22] However, the use of LbL technique in polymer hybrid solar cells has been very limited. In this study, we applied

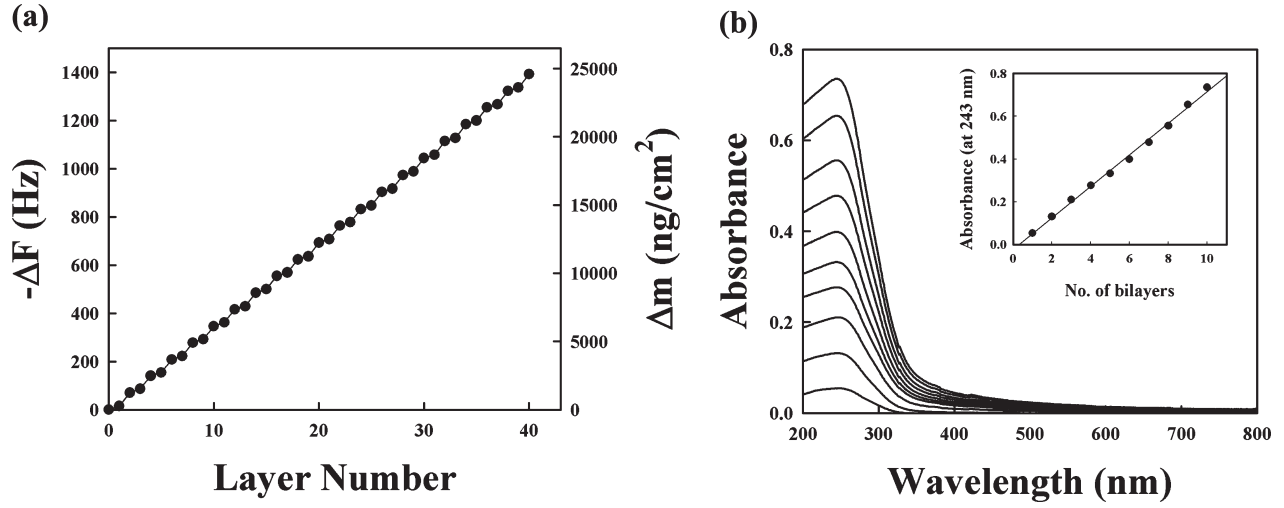

Figure 1. (a) Frequency and mass change of PAH/TALH multilayers measured with increasing layer number from 1 to 40. In this case, the mass change per unit area was calculated from frequency change. (b) UV−vis absorbance spectra of $(PAH/TALH)_n$ multilayers measured with increasing bilayer number (n) from 1 to 10.

the LbL method to fabricate TiO_xNC as the electron acceptor in photovoltaic cells. To investigate the specific effect of LbL TiO_xNC on device performance and compare the LbL material directly to the sol−gel TiO_xNC layer, photovoltaics were fabricated using the bilayer (i.e., ITO/TiO_x/P3HT/Ag). Although the inherent efficiency of the bilayer device was not high because of the very short exciton diffusion length of 5−10 nm in conjugated polymers,[32,33] the simple device structure with a well-defined interface between electron donor and acceptor made it simple to investigate the optoelectronic properties of LbL TiO_xNC in our study. When the conducting polymer was used as the electron donor in bilayer type solar cells, a regioregular P3HT polymer with high hole mobility and well-ordered 2D-packing structure was synthesized by the modified McCoullough method.[34−37]

Figure 2 represents the current density versus voltage ($J-V$) curves for the LbL processed TiO_x/P3HT and the sol−gel TiO_x/P3HT devices, illuminated under air mass (AM) 1.5 conditions. The solar cell based on sol−gel TiO_x/P3HT active layers displayed a short-circuit current density (J_{sc}) of 0.45 mA/cm^2, an open-circuit voltage (V_{oc}) of 0.47, a fill factor (FF) of 0.38, and a power conversion efficiency (PCE) of about 0.08%. On the other hand, under the same white light illumination, the cell composed of LbL TiO_xNC/P3HT showed significantly improved device performance (i.e., J_{sc} of 0.72 mA/cm^2, V_{oc} of 0.57, FF of 0.62, and PCE of 0.25%) compared to that of the sol−gel TiO_x-based devices. Table 1 summarizes the device characteristics for these devices. These results are significant given that these two devices have identical device structures and layer thicknesses. A major portion of the enhancement is attributed to the increase in FF and J_{sc}, which could be induced by the effective electron/hole transfer between the interfaces of the hybrid layers (i.e., P3HT and LbL TiO_xNC) and furthermore the charge transport within the cells.

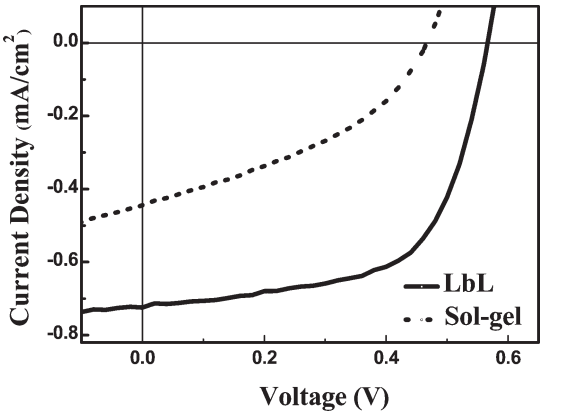

Figure 2. Current density−voltage measurements of two different P3HT/TiO_x solar cells under AM 1.5G illumination (100 mW/cm^2).

Table 1. Device Characteristics of Two Different TiO_x/P3HT Solar Cells under AM 1.5G Illumination (100 mW/cm^2)

type of TiO_x	thickness (nm)	V_{oc} (V)	J_{sc} (mA/cm^2)	FF	PCE (%)
sol−gel	50	0.47	0.45	0.38	0.08
LbL	50	0.57	0.72	0.62	0.25

The increase in the interfacial area between conjugated polymers and TiO_x layers has been reported to enhance the power conversion efficiency of solar cells by collecting more excitons at the interface.[20−22] Therefore, we first investigated the surface morphology of two different LbL and sol−gel TiO_xNC films using tapping mode AFM as shown in Figure 3. In this case, the root-mean-square (rms) surface roughnesses of LbL and sol−gel TiO_x films were measured as about 0.55 and 0.53 nm, respectively. The similar surface roughness values between the two different types of TiO_x films cannot explain the dramatic enhancement observed for the P3HT/LbL TiO_x solar cell device.

Another possibility is that the chemical composition of LbL TiO_xNC has a positive effect on the interfacial properties between the P3HT and TiO_x layers and thus improves the device performance. The interfacial properties of TiO_x layers are one of the critical factors determining the device performance due to their effect on the electron transfer between the polymers and TiO_x

(32) Savenije, T. J.; Warman, J. M.; Goossens, A. *Chem. Phys. Lett.* **1998**, *287*, 148.
(33) Liu, Y.; Summers, M. A.; Edder, C.; Fréchet, J. M. J.; McGehee, M. D. *Adv. Mater.* **2005**, *17*, 2960.
(34) Liu, J.; McCullough, R. D. *Macromolecules* **2002**, *35*, 9882.
(35) Miyakoshi, R.; Yokoyama, A.; Yokozawa, T. *J. Am. Chem. Soc.* **2005**, *127*, 17542.
(36) Sheina, E. E.; Liu, J.; Iovu, M. C.; Laird, D. W.; McCullough, R. D. *Macromolecules* **2004**, *37*, 3526.
(37) Kim, B. J.; Miyamoto, Y.; Ma, B.; Fréchet, J. M. J. *Adv. Funct. Mater.* **2009**, *19*, 2273.

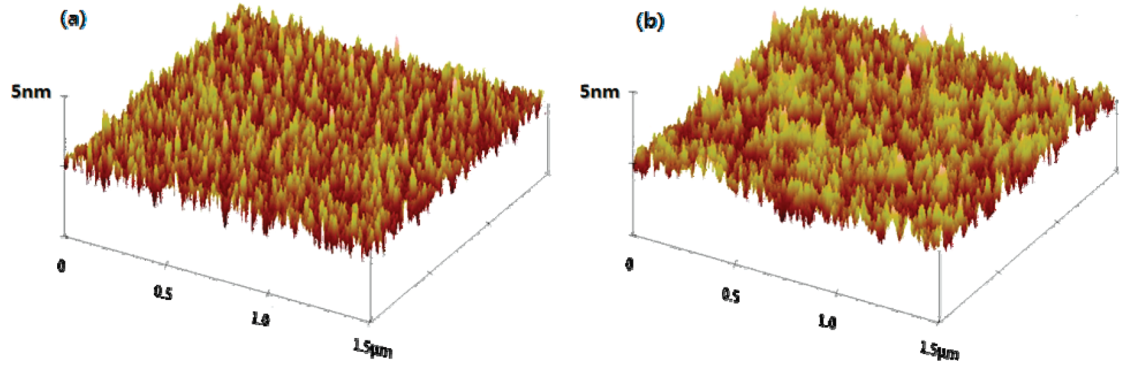

Figure 3. Tapping mode AFM topography images of (a) LbL and (b) sol−gel TiO_xNC surface showing the rms surface roughnesses of about 0.55 and 0.53 nm, respectively. The scan size was 1.5 μm × 1.5 μm.

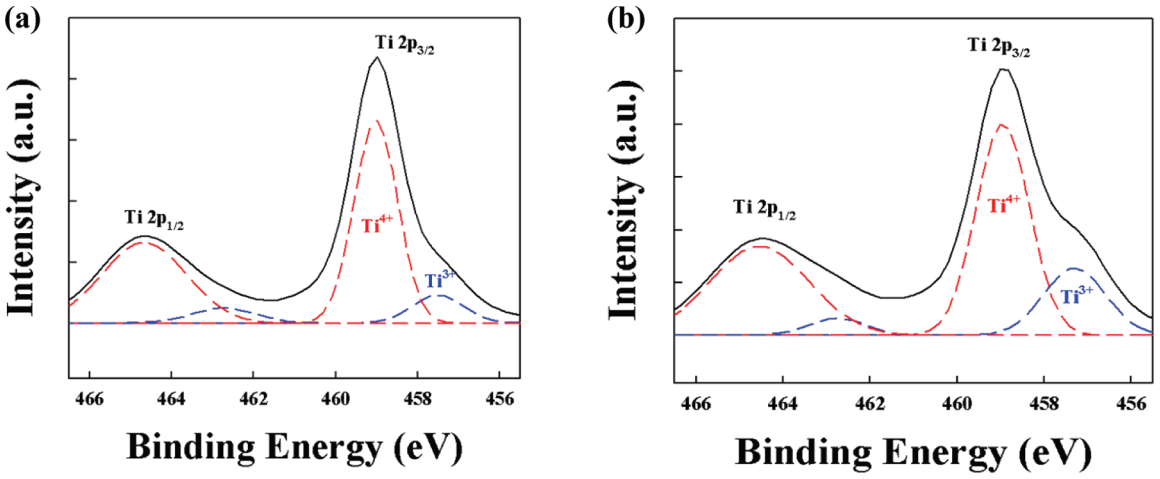

Figure 4. X-ray photon spectroscopy spectra of (a) sol−gel TiO_x films (Ti^{3+}/Ti^{4+} ratio = 0.16) and (b) LbL TiO_xNC films (Ti^{3+}/Ti^{4+} ratio = 0.37).

layers as well as the hole mobility and the structural order of the conjugated polymer film.[12,38] To confirm this possibility, the chemical compositions of two different types of TiO_x surfaces were investigated by XPS analysis. The initial thermal annealing process under nitrogen can induce oxygen deficiencies accompanied by an increase in the local electron concentration. This oxygen-deficient state can be confirmed by the Ti $2p_{3/2}$ peak shifting to a lower binding energy due to the presence of Ti^{3+} ions. The measured spectrum can be resolved into two spin−orbit components, which are identified as Ti^{4+} (459.2 eV) and Ti^{3+} (457.8 eV). As shown in Figure 4a,b, the difference in the Ti^{3+}/Ti^{4+} ratio between the two layers is significant, demonstrating that LbL TiO_xNC samples have a Ti^{3+}/Ti^{4+} ratio of 0.37, which is more than 2 times higher than that of the sol−gel TiO_x samples. Because Ti^{3+} ions or oxygen vacancies act as electrically conducting semiconductors, the two different P3HT/TiO_x (sol−gel and LbL) devices are expected to have different interfacial properties, thus affecting the electron transfer between the electron donor and acceptor layers. According to previous reports,[39,40] since the oxygen-deficient Ti^{3+} states in TiO_x form a donor level between the bandgaps of TiO_x, the Ti^{3+} surface states can trap the photogenerated electrons and then transfer them to O_2 adsorbed on the surface of TiO_x. Therefore, the existence of the Ti^{3+} surface states in TiO_x results in reduced rates of electron and hole recombination, which definitely has a positive effect on the solar cell performance. Other groups also reported the crucial and beneficial effect of oxygens on the polymer/TiO_x hybrid solar cells. They claimed that the role of oxygen makes the oxide surface electron deficient and keeps the oxide as an efficient electron acceptor, thus enhancing device performance.[41,42]

Furthermore, X-ray diffraction (XRD) was also performed to examine the formation and crystalline structure of the sol−gel TiO_x and LbL TiO_x NC after thermal annealing at 450 °C. As shown in Figure 5a,b, the XRD pattern of the sol−gel TiO_x formed after thermal annealing displayed an evident (101) plane peak typical of anatase crystals, which are thermodynamically stable. On the other hand, a (001) plane peak was dominant in the LbL TiO_xNC films, which is a signature of highly reactive facets of the anatase TiO_x crystals.[43,44] The structure shown in LbL TiO_xNC films is closely related to the crystalline growth of TALH layers confined between the adjacent PAH layers. In addition, bright field transmission electron microscopy (TEM) images taken from the cross-sectional area of the sol−gel, and LbL TiO_xNC films confirm the findings of XRD measurements, showing that (001) crystalline peaks are only predominant in the LbL TiO_xNC films. For the same anatase type TiO_x, both theoretical

(38) Lloyd, M. T.; Prasankumar, R. P.; Sinclair, M. B.; Mayer, A. C.; Olson, D. C.; Hsu, J. W. P. *J. Mater. Chem.* **2009**, *19*, 4609.
(39) Yu, J. G.; Zhao, X. J.; Zhao, Q. N. *Mater. Chem. Phys.* **2001**, *69*, 25.
(40) Yu, J. C.; Yu, J.; Ho, W.; Jiang, Z.; Zhang, L. *Chem. Mater.* **2002**, *14*, 3808.
(41) Lira-Cantu, M.; Norrman, K.; Andreasen, J. W.; Krebs, F. C. *Chem. Mater.* **2006**, *18*, 5684.
(42) Greene, L. E.; Law, M.; Yuhas, B. D.; Yang, P. D. *J. Phys. Chem. C* **2007**, *111*, 18451.
(43) Yang, H. G.; Sun, C. H.; Qiao, S. Z.; Zou, J.; Liu, G.; Smith, S. C.; Cheng, H. M.; Lu, G. Q. *Nature* **2008**, *453*, 638.
(44) Dai, Y. Q.; Cobley, C. M.; Zeng, J.; Sun, Y. M.; Xia, Y. N. *Nano Lett.* **2009**, *9*, 2455.

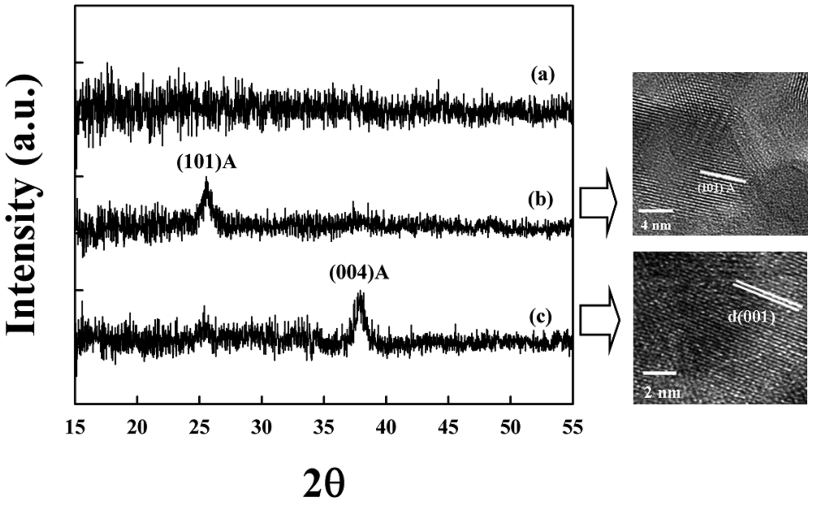

Figure 5. XRD spectra of (a) sol−gel TiO_x film before thermal annealing, (b) sol−gel TiO_x film after thermal annealing at 450 °C, and (c) LbL TiO_xNC film after thermal annealing at 450 °C. High-resolution TEM images represent TiO_xNC crystalline structures taken from the cross-sectional area of the corresponding (b) sol−gel and (c) LbL TiO_xNC crystalline structures, respectively.

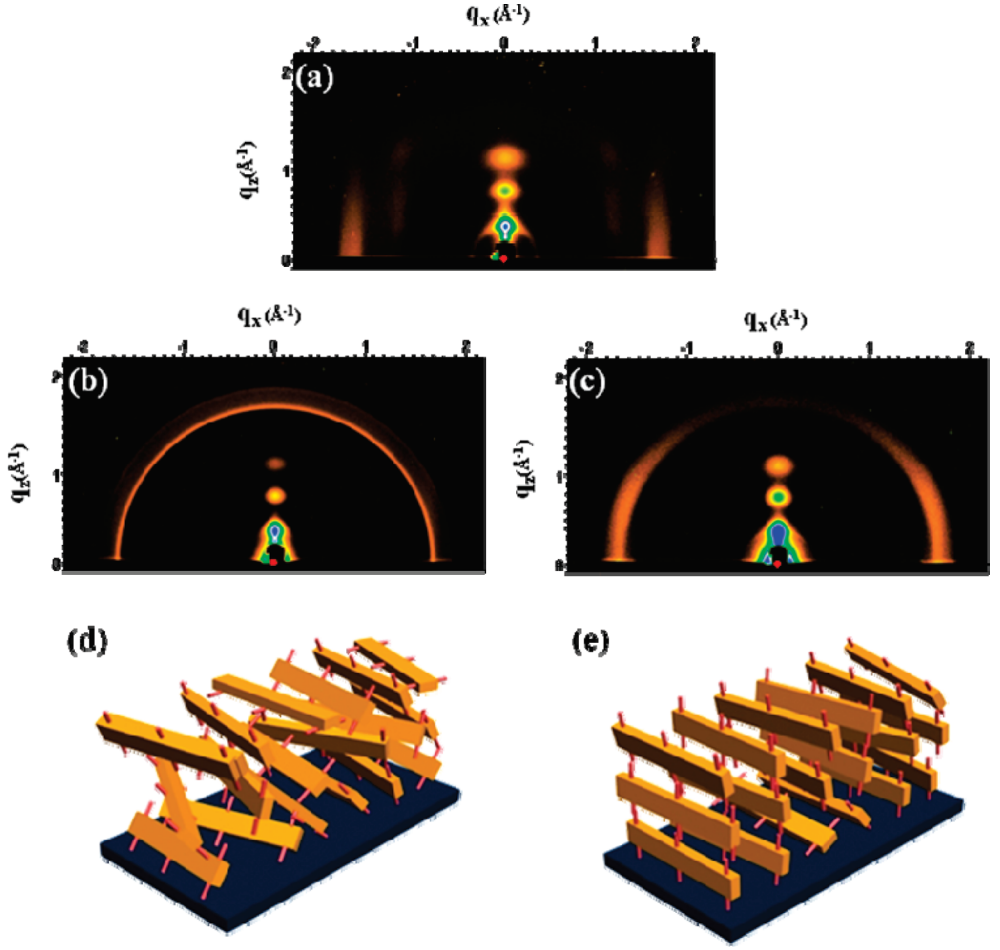

Figure 6. GIWAXS patterns of ∼10 nm thick P3HT films on (a) Si substrate, (b) sol−gel TiO_xNC film, and (c) LbL TiO_xNC film. All samples are annealed at 120 °C for 8 h. Parts (d) and (e) represent the schematic illustration of P3HT stacks on the sol−gel and LbL TiO_xNC films, respectively.

and experimental studies have found that the (001) planes are much more reactive compared to the (101) planes.[45] And it was reported by Besenbacher's group that the oxygen molecules adsorbed on the TiO_x surface, which acts as electron trap that delays electron−hole pair recombination, are diffused only along (001) surface.[46] Therefore, the reactive sites of LbL TiO_xNC combined with the existence of a larger number of Ti^{3+} surface states can suppresses

(45) Gong, X. Q.; Selloni, A. *J. Phys. Chem. B* **2005**, *109*, 19560.

(46) Wahlstrom, E.; Vestergaard, E. K.; Schaub, R.; Ronnau, A.; Vestergaard, M.; Laegsgaard, E.; Stensgaard, I.; Besenbacher, F. *Science* **2004**, *303*, 511.

the electron−hole recombination, thus resulting in higher short-circuit density and fill factor.

A deeper insight into the dramatic difference observed in photovoltaic performance can be gleaned by examination of the 2-dimensional structure of the P3HT film near the P3HT/TiO_x interface via grazing incidence wide-angle X-ray scattering (GIWAXS). Since the few nanometer range P3HT crystalline structure is one of the critical factors controlling charge transport and charge transfer from the polymer to the inorganic electron acceptor,[38] we prepared very thin P3HT films (~10 nm) on three different substrates. Figure 6b represents a GIWAXS pattern of a 10 nm thick P3HT film prepared on the sol−gel TiO_xNC substrates, and Figure 6c shows a GIWAXS pattern of a 10 nm thick P3HT film on the LbL TiO_xNC substrates. For reference, a 10 nm thick P3HT film was prepared identically but on a Si substrate, as shown in Figure 6a.

Each of the 2D image maps of GIWAXS patterns in Figure 6 can be divided into a component in the plane of the substrate (q_x) and a component perpendicular to the substrate (q_z). In the reference sample as shown in Figure 6a, the (100), (200), and (300) diffraction peaks of P3HT peaks are strongest in the out-of-plane direction, indicating that after thermal annealing at 120 °C for 8 h, the P3HT films have a well-organized structure with planar P3HT stacks oriented along an axis perpendicular to the substrate. And (100), (200), and (300) peak positions of P3HT polymers on Si substrate were found at 1.695, 0.847, and 0.559 nm, respectively, indicating that the distance between adjacent P3HT alkyl chains is ~1.69 nm. It is very noticeable that the peak at 0.38 nm is found only in in-plane direction with very strong streak pattern, indicating that the $\pi-\pi$ stacking between P3HT chains are highly oriented along an axis parallel to the substrate. This is typical of high crystalline regioregular P3HT films.[47,48]

In stark contrast, the peak at 0.38 nm in Figure 6b was randomly oriented in all different directions, indicating that the orientation of the P3HT $\pi-\pi$ stacking in the film on the sol−gel TiO_xNC substrate was randomly distributed. On the other hand, Figure 6c shows that the peak of the $\pi-\pi$ stacking between P3HT chains was much stronger in the in-plane direction than in the out-of-plane direction, indicating that the $\pi-\pi$ stacking between P3HT chains was well-oriented parallel to the substrate and only a few domains were aligned with the (010) direction perpendicular to the substrate. Although the $\pi-\pi$ stacking distances in the LbL and sol−gel TiO_xNC layers were found to be exactly 0.38 nm, the preferential stacking direction was very different between two samples, which could be a critical factor controlling the charge mobility of P3HT and the charge transfer between the P3HT and TiO_x layers.[49,50] For example, disoriented P3HT $\pi-\pi$ stacking observed in the sol−gel TiO_x film can have more defects and disordered boundaries between crystalline P3HT domains, which are detrimental to the charge transport properties of the P3HT films.[47,51] And a better ordering of crystalline domain of P3HT stacks on the LbL TiO_xNC films can enhance the charge mobility.[52] Furthermore, according to the previous reference,[53] the highly oriented $\pi-\pi$ stacking near and at the P3HT/interface may increase the exciton diffusion and therefore enhance charge generation at the interface. We believe that the difference in the surface properties between the two different TiO_x layers observed by XPS and XRD measurements induced the change in the two-dimensional structure of P3HT chains and the orientation of their $\pi-\pi$ stacking on the TiO_x film. The specific effect of the P3HT structure and ordering on the electronic properties of the solar cells is under further investigation by high-resolution X-ray scattering and other techniques.

Conclusions

In summary, this work demonstrates that the LbL TiO_xNC film is of value in the preparation of polymer−inorganic hybrid solar cells. An evident advantage of the LbL method in the preparation of TiO_xNC films is that the chemical composition and nanostructures of LbL TiO_xNC can be controlled to be suitable for photovoltaic applications. In the model system of P3HT/TiO_x bilayer solar cells, the short-circuit current and fill factor in the P3HT/LbL TiO_xNC cells were greatly enhanced compared to those in P3HT/sol−gel TiO_xNC, thus resulting in a 3-fold increase in the power conversion efficiency. XPS measurements revealed that the LbL TiO_xNC films retained a 2 times higher Ti^{3+}/Ti^{4+} ratio than the sol−gel TiO_x samples, suppressing the electron and hole recombination rates and thus facilitating the electron transfer between the electron donor and acceptor. Furthermore, differences in crystalline nature between the LbL and sol−gel TiO_xNC films were clearly observed by XRD and TEM. In addition, GIWAXS results indicated that the P3HT $\pi-\pi$ stackings were better oriented to the substrate in the LbL TiO_xNC/P3HT films, which also contributed to the dramatic improvement in the PCE of the solar cells. This study demonstrated a facile and versatile method to improve the performance of polymer/inorganic hybrid solar cells by tuning the chemical and interfacial properties of TiO_xNC. Furthermore, this work establishes some of the fundamental rules for the design of inorganic electronic acceptor materials that can be used broadly in other electronic applications, including photovoltaic devices.

Acknowledgment. This research was supported by the Korea Research Foundation Grant funded by the Korean Government (MOEHRD) (2009-0085070, 2009-0088551, 2010-0011033, 2010-0029106), EEWS Research Project of the office of KAIST EEWS Initiative (EEWS-2010-N01100039), and the New & Renewable Energy of the KETEP grant funded by the Ministry of Knowledge Economy, Korea (2010-T100100460). The authors thank Mr. Myungsun Sim for the help in GIXS measurements at Pohang Synchrotron Light Source.

(47) Kim, Y.; Cook, S.; Tuladhar, S. M.; Choulis, S. A.; Nelson, J.; Durrant, J. R.; Bradley, D. D. C.; Giles, M.; Mcculloch, I.; Ha, C. S.; Ree, M. *Nature Mater.* **2006**, *5*, 197.

(48) Kline, R. J.; Mcgehee, M. D.; Toney, M. F. *Nature Mater.* **2006**, *5*, 222.

(49) McCulloch, I.; Heeney, M.; Chabinyc, M. L.; DeLongchamp, D.; Kline, R. J.; Coelle, M.; Duffy, W.; Fischer, D.; Gundlach, D.; Hamadani, B.; Hamilton, R.; Richter, L.; Salleo, A.; Shkunov, M.; Sporrowe, D.; Tierney, S.; Zhong, W. *Adv. Mater.* **2009**, *21*, 1091.

(50) Salleo, A.; Kline, R. J.; Delongchamp, D. M.; Chabinyc, M. L. *Adv. Mater.* **2010**, *22*, 3812.

(51) Kline, R. J.; McGehee, M. D.; Kadnikova, E. N.; Liu, J. S.; Fréchet, J. M. J.; Toney, M. F. *Macromolecules* **2005**, *38*, 3312.

(52) Redecker, M.; Bradley, D. D. C.; Inbasekaran, M.; Woo, E. P. *Appl. Phys. Lett.* **1999**, *74*, 1400.

(53) Ravirajan, P.; Bradley, D. D. C.; Nelson, J.; Haque, S. A.; Durrant, J. R.; Smit, H. J. P.; Kroon, J. M. *Appl. Phys. Lett.* **2005**, *86*, 143101.